Published in final edited form as:
Bioorg Med Chem. 2013 August 1; 21(15): 4678–4686. doi:10.1016/j.bmc.2013.05.018.

Protective activity of (1*S*,2*E*,4*R*,6*R*,7*E*,11*E*)-2,7,11-cembratriene-4,6-diol analogues against diisopropylfluorophosphate neurotoxicity: Preliminary structure-activity relationship and pharmacophore modeling

Vesna A. Eterović[a,*], **Angelie Del Valle-Rodriguez**[a], **Dinely Pérez**[a], **Marimée Carrasco**[a], **Mohammad A. Khanfar**[b], **Khalid A. El Sayed**[c,*], and **Pedro A. Ferchmin**[a]

[a]Department of Biochemistry, School of Medicine, Universidad Central del Caribe, Bayamón, PR 00960, USA

[b]Department of Basic Pharmaceutical Sciences, Faculty of Pharmacy, The University of Jordan, Amman, 11942, Jordan

[c]Department of Basic Pharmaceutical Sciences, College of Pharmacy, University of Louisiana at Monroe, Monroe, LA, 71201, USA

Abstract

Diisopropylfluorophosphate (DFP) is an organophosphorous insecticide used as a surrogate for the more toxic chemical warfare nerve agent sarin. DFP produces neurotoxicity *in vivo* and irreversibly decreases the area of population spikes recorded from the CA1 region of acute hippocampal slices. (1*S*,2*E*,4*R*,6*R*,7*E*,11*E*)-2,7,11-Cembratriene-4,6-diol (**1**) is a neuroprotective natural cembranoid that reverses DFP-induced damage both *in vivo* and in the hippocampal slice. Cembranoid **1** acts by noncompetitive inhibition of the α7 nicotinic acetylcholine receptor. This study aims at establishing a preliminary structure-activity relationship to define the neuroprotective cembranoid pharmacophores using the hippocampal slice assay and pharmacophore modeling. Fourteen natural, semisyntheti or biocatalytic cembranoid analogues **2**-**15** related to **1** were tested for their capacity to protect the population spikes from DFP-induced damage and intrinsic toxicity. Twelve cembranoids caused significant reversal of DFP toxicity; only 3 active analogues displayed minor intrinsic toxicity at 10 μM. The C-4 epimer of **1** (**2**) and the 4-*O*-methyl ether analogue of **1** (**3**), were totally devoid of neuroprotective activity. The results suggested a model for cembranoid binding where the hydrophobic ring surface binds to a hydrophobic (Hbic) patch on the receptor molecule and an electronegative atom (oxygen or sulfur) in proper spatial relationship to the ring surface interacts with an electropositive group in the receptor binding site. A pharmacophore model consisting of 1 hydrogen bond acceptor (HBA), 2 Hbic, and 10 exclusion spheres was established using HipHop-REFINE and supported the above mentioned pharmacophoric hypothesis.

*To whom Correspondence should be addressed. KA El Sayed (Medicinal Chemistry) Telephone 318-342-1725. Fax: 318-342-1737. elsayed@ulm.edu, VA Eterovic (Biology) Telephone 787-798-3001 X2032. Fax: 787-786-6285 vesna.eterovic@gmail.com.

A. Supplementary data: Supplementary data associated with this article can be found, in the online version, at doi:xxxx. These data include NMR data of compounds **1**-**15** and EC_{50} data of **1**, **2**, **6**, **7**, **10**, and **15**.

Keywords

DFP; Neuroprotection; Neurotoxicity; Organophosphorous insecticide; Pharmacophore modeling; Tobacco cembranoids

1. Introduction

Organophosphates (OPs) are a diverse family of chemicals used in industry, agriculture, medicine and warfare. Examples include chemical war nerve agents (soman, sarin, tabun, VX) and insecticides (malathion, parathion, chlorpyrifos). OP's are readily absorbed by inhalation, ingestion and skin penetration and represent a serious health problem.[1,2] Since toxic OP's are difficult to handle in the research laboratory, less noxious OP's are used instead. Thus, diisopropylfluorophosphate (DFP) is used in research as a surrogate for the nerve gas sarin.

Many neurotoxic OPs, DFP included, inhibit acetylcholinesterase (AChE) and the resultant accumulation of acetylcholine (ACh) causes a muscarinic and, to a lesser degree, a nicotinic crisis that is often fatal.[3] In brain, DFP induces a prolonged Ca^{2+} plateau and excitotoxicity,[4] which leads to neuronal death. Delayed neurological deficiencies in survivors of OPs exposure were reported in many cases.[5] Present therapies do not address the last problem. Therefore, there is an urgent need for antidotes with neuroprotective activity that arrest the delayed apoptotic neuronal damage.

We have discussed previously the merits of the acute hippocampal slice as the model for neurodegeneration and neuroprotection.[6-7] The size of the population spike (PS) is directly proportional to the number of functionally active pyramidal neurons[8], thus quantification of PS area provides a measure of the number of damaged neurons. Furthermore, the decrease in PS area is related to the initiation of apoptosis because it does not occur in the presence of a cell permeable inhibitor of caspase 9;[9] activation of caspase 9 is an early step in the intrinsic apoptotic pathway.[10]

(1*S*,2*E*,4*R*,6*R*,7*E*,11 *E*)-2,7,11-Cembratriene-4,6-diol (**1**) (Figure 1) is a cyclic diterpenoid that displays neuroprotective activity *in vivo* and *ex vivo* rat models.[6,7,11-14] In the acute hippocampal slice preparation, **1** rescues the PSs from NMDA-induced damage,[7,12] as well as from two neurotoxic OPs: paraoxon[6] and DFP.[13] All three toxic stimuli, NMDA, paraoxon and DFP, decreased the PS area in a concentration and time-dependent manner while post-application of **1** reversed the toxic effect. Cembranoid **1** rescued the PS by triggering an antiapoptotic mechanism through noncompetitive inhibition of the α7 nicotinic acetylcholine receptor (α7); inhibition of the α7 receptor indirectly caused the activation of Akt/PKB in pyramidal neurons.[12] We also reported that **1** inhibited the activity of human α7 nAChR heterologously expressed in SHSY5Y cells.[7]

The objective of this study was to establish a preliminary SAR and define the pharmacophoric features of cembranoids that are necessary for neuroprotection without intrinsic toxicity, using the hippocampal slice assay and pharmacophore modeling. The long-term objective is the identification of a diverse library of cembranoid-inspired synthetic or semisynthetic analogues appropriate for future lead optimization studies for use as drug antidotes against organophosphorous-induced neurodegeneration.

2. Results and discussion

Fourteen natural, semisynthetic, or biocatalytic cembranoid analogues **2**-**15** related to **1** (Figure 1) were tested for their capacity to protect the PSs from DFP-induced damage and

intrinsic toxicity. There were three treatment groups: 1) the *DFP control group* tested for the toxic effect of DFP defined as the decrease of PS area upon exposure of the slices to 100 μM DFP for 10 min; 2) *Cembranoid protective activity group* measured cembranoid capacity to reverse DFP toxicity by following the exposure to DFP with a 30 min washout followed by exposure to 10 μM cembranoid for 1 h; and 3) *Cembranoid toxicity control* tested for a possible toxic effect of the cembranoid upon exposure of the slice to 10 μM cembranoid for 1 h (Figure 2). For each group, PSs were recorded from 7 slices before (initial PS) and after treatment (final PS). Separate experiments were done to determine the rundown of slices exposed for 2 h to the ACSF buffer (*ACSF control*).

Figure 3 exemplifies the PSs recorded before and after exposure of the slice to the various treatments used in this work. The PS was not significantly reduced upon exposure of the slice to the standard artificial cerebrospinal fluid (ACSF), **1** or **2** (Figures 3A-3C). The PS was significantly reduced upon incubation with 100 μM DFP for 10 min, which indicated that DFP was toxic to the slice (Figure 3D). However, when exposure to DFP was followed by superperfusion with 10 μM **1**, the PS area returned to the level observed with slices not exposed to DFP (Figure 3E). The EC_{50} value of **1** was proved 63+9 nM, with 83% maximum recovery at 10 μM (Table 1). On the contrary, superfusing the slice with 10 μM of the 4-epi-analogue of **1** (cembranoid **2**) after DFP did not rescue the PS (Figure 3F).

Figure 4 summarizes the results for all compounds tested. We will first discuss the data from the *ACSF control* and the *Cembranoid toxicity control* groups (white and hatched bars, Figure 4). Upon exposure of the slice to ACSF for two hours, the PS showed an average 10% rundown. Therefore, cembranoid % recovery was compared to the 90% value expected from the normal rundown. Eleven out of the fifteen tested cembranoids did not show a rundown significantly larger than that expected in the absence of cembranoid, which indicated lack of toxicity. Cembranoids **6, 12, 10** and **2** displayed minor toxicity, showing 75-81% recovery as compared to 90% for the ACSF control ($p<0.05$). On the other hand, application of DFP reduced the PS area to 20-40% of the initial PS value *(DFP control*, black bars, Figure 4); this effect persisted after a two-hour washout period and was highly significant for each individual experiment ($p<0.001$).

The effect of cembranoids applied after DFP is indicated with gray bars on Figure. 4. When 10 μM of **1** was applied 30 min after DFP, a dramatic reversal of DFP toxicity from 28% to 86% recovery was observed ($p<0.01$). Analogues **4**-**6** and **8**-**15** all reversed DFP toxicity to a degree similar to that observed with **1**. In every case, the % recovery observed after exposure to DFP plus cembranoid was significantly larger than that observed after exposure to DFP alone ($p<0.01$) but not significantly different from that observed after exposure to cembranoid alone. This last observation indicated that the recovery was essentially complete. A recovery of 70±6% was observed with DFP plus **7**, versus 101±10% after **7** alone ($p<0.05$), with EC_{50} value of 14+2 nM (Table 1), which indicated incomplete recovery. No protective activity was observed with analogues **3** and **2**. Thus, at 10 μM concentration, 12 out of 15 cembranoids tested caused complete reversal of DFP toxicity while two displayed complete loss of protective activity.

The neuroprotective activity of cembranoids **1**-**15** can then be categorized into two main groups (Figure 1): those affording protection similar to the parent compound **1** (Figures 1A and 1C) and those showed complete activity loss, namely **2** and **3** (Figure 1B). These results allowed the speculation of the molecular features that underlay cembranoids' protective activity. First, hydroxylation at carbons C-9, C-10, C-19 and C-20 (**9**-**13**) or oxidation of C-6 hydroxyl to a keto group (**8**) preserved full neuroprotective activity of **1**. The EC_{50} value of **10** was found to be 87+36 nM with 76% maximal recovery at 10 μM (Table 1). Furthermore, cembranoid **15**, with the cyclized 2H-thiopyran ring was entirely chemically

different from other cembranoids and yet preserved the protective activity. The EC_{50} value of **15** was found to be 31±1 nM with 85% maximal recovery at 10μM (Table 1). Second, it is evident that the *R*-chirality of carbon C-4 is required for activity based on the complete activity loss when C-4 chirality is inverted to C-4*S* as in **2**. A free -hydroxy at C-4 was important for the cembranoids' activity since the effect was lost by methylation of C-4 hydroxy as in **3**. Third, the carbonyl at C-6 restored the lost activity of the 4-*O*-methyl ether **3** (cf. **4** and **14** with **3**). The ^{2,3} geometry was not critical for activity as suggested by the potent activity of both the *E*-and *Z*-oriented ^{2,3} in **4** and **14**, respectively. The C-11*S*,12*S*-epoxy functionality also rescued the activity of **3** as suggested by the activity of its 11,12-epoxy analogues **5** and **6**. The C-6-*O*-acetate in **6** did not affect the activity of **5**. The EC_{50} value of **6** was found to be 277±87 nM with 88% maximal recovery at 10μM (Table 1). The C-7*R*,8*S*-epoxy present in **7** partially rescued the activity of **3**.

Figure 5 illustrates the 3D energy-minimized structures of cembranoids. The parent cembranoid **1** (Figure 5A) consists of a rather flat hydrophobic surface formed by the 14-carbon macrocyclic ring and two electronegative oxygen atoms close to the ring upper border: the C-4 - and the C-6 - hydroxy oxygens aligned above and below the ring surface plane, respectively. Both structural modifications that produced complete loss of activity, namely epimerization of the *C*-4*R* stereoisomer to *C*-4*S* and methylation of C-4 hydroxy, introduced conformational changes that were restricted to the C-4 position (Figure 5B). These observations are consistent with the following model for cembranoid binding: the hydrophobic ring (or a portion of it) interacts with a hydrophobic patch or pocket in the receptor binding site, while the electronegative oxygen on C-4 - position interacts with complementary group(s) on the receptor. This could entail the formation of a hydrogen bond where the C-4 hydroxy group either donates the hydrogen or accepts electrons from the receptor. The change to C-4*S* chirality moves the C-4 oxygen away from its complementary group(s) on the receptor. Methylation, on the other hand, blocks the hydrogen bonding donor ability of this hydroxyl group (if it were assumed that this hydroxyl group acted as a hydrogen donor); or, methylation could decrease oxygen electronegativity and interfere with oxygen's approach to the receptors hydrogen.

Hydroxylation at carbons C-9 (-OH), C-10 (- or -OH), C-19 and C-20 (cembranoids **9**-**13**) did not affect ring conformation or the relative stereo-orientation of the C-4 and C-6 substituents. These observations are consistent with the proposed model since the C-4 oxygen and the hydrophobic ring plane are not affected by these substitutions (Figure 5C). Oxidation of C-6 hydroxy to a keto group (as in **4**, **8** and **14**) increases the rigidity of the segment C-4-C-6 and moves the C-6 toward the front side of the ring bringing the ketone oxygen into proximity of the C-4 hydroxy, while the rest of the macrocycle carbons remain basically the same (Figure 5D). It is therefore conceivable that the C-6 keto could replace the C-4 hydroxy, acting as a hydrogen bond acceptor. In cembranoids **4** and **14**, binding of the 6-keto could rescue the activity that was lost by methylation of C-4 hydroxy (as in **3**). The *Z*-double bond geometry of ^{2,3} in **14** introduces significant changes in ring conformation, but the features of the hydrophobic plane and the electronegative oxygens in proper spatial relationship, are preserved (Figure 5D). The model also explains the rescue of activity by the 11*S*,12*S*-epoxy functionality. Figure 5E illustrates that a horizontal flip of **5** brings the epoxy oxygen to the position of the C-4 oxygen in **1**. The relative position of this oxygen and the hydrophobic surface is preserved, although the cembranoid is now presumed to bind with the “rear” surface of the ring. The C-6-*O*-acetate in **6**, which did not affect the protective activity of **5**, is shown out of the way of the binding groups. The 7*R*,8*S*-epoxy functionality present in **7** introduced a significant change in the conformation of the ring. When the epoxy oxygen is forced to coincide with the C-4 hydroxy of **1**, it becomes evident that the shape of the hydrophobic surface is changed considerably, presumably decreasing

the binding surface. This is consistent with this cembranoid decreased potency. Finally, the 3D structure of **15** indicates that the electronegative S atom occupies a position similar to the C-4 oxygen of **1**, and could therefore serve the same purpose, e.g., acting as a hydrogen bond acceptor (Figure 5F). Therefore, a model assuming that cembranoids binding involves the hydrophobic macrocycle ring surface and an electronegative atom (O or S) located at an optimal position near the ring border is consistent with the results found in this study.

To further confirm the abovementioned cembranoid SAR model, we employed the HipHop module of CATALYST software to build reasonable binding hypotheses. The fifteen cembranoids **1**-**15** were used as a training set for pharmacophore modeling (Table 2). A conformational database for each of the training compounds was generated using the 'Best' option. HipHop identifies 3D spatial arrangements of chemical features that are common to active structures in a training set. Principal and MaxOmitFeat parameters define how many structures must map completely or partially to the hypothesis. After several trials, it was decided to configure HipHop as follows: cembranoids **1**, **4**-**6**, and **8**-**15**, which showed significant reversal of DFP toxicity were assigned a Principal Value of 2 and MaxOmitFeat of zero (Table 2) to ensure that all of the chemical features in these compounds will be considered in building the pharmacophore space. Cembranoid **7**, which showed incomplete recovery of DFP toxicity, was assigned a Principal Value of 1 (Table 2) to ensure that it will be mapped at least once by each generated hypothesis, and allowed to miss one feature in any generated model by assigning it a MaxOmitFeat parameter of one (Table 2). On the other hand, cembranoids **2** and **3**, which are devoid of protective activity, were assigned a Principal Value of zero and MaxOmitFeat of 2. Based on cembranoid structures, HipHop was asked to explore up to 5-featured pharmacophoric space of the following possible features: HBDs, HBAs, and Hbic. Moreover, the number of features of any particular type was allowed to vary from 0 to 3 for HBA, 0 to 1 for HBD and 0 to for Hbic. Finally, HipHop was constructed to permit a minimal inter-feature distance of 1 Å to build the hypothesis. Ultimately, 10 optimal pharmacophoric hypotheses were created. The generated hypotheses share the same number of features; 1 HBA, 2 to 3 Hbic, and variable number of exclusion spheres but with different 3D spatial arrangements. The highest ranked pharmacophore model is shown in Figure 6 mapped against compounds **1**, **4**, **5**, and **15**. This model which consists of 1 HBA, 2 Hbic, and 10 exclusion spheres support the SAR discussed above. The two Hbic features facing the macrocycle ring support the need for hydrophobic surface required for binding to a hydrophobic pocket(s) on the receptor. On the other hand, the vectored HBA feature can explain the necessity for an electronegative atom to interact with an electropositive atom (or group) in the receptor binding site through dipole-dipole or hydrogen bonding interaction. This model explained how the loss of protective activity by methylation or elimination of C-4 hydroxyl group could be recovered by a keto group on carbon 6 (compounds **4** and **14**), epoxy group in 11*S*,12*S* or 7*R*,8*S* positions (compounds **5**-**7**), or introduction of a new atom (compound **15**). Figures 6B-6D describe how the C-6 keto group of **4**, the epoxy group of **5**, and S atom of **15**, respectively, occupy the same position of the C-4 hydroxyl group of **1** and act as HBA. The hydroxyl groups at positions C-9 (β-OH), C-10 (β- or α-OH), C-19, and C-20 were not essential for protective activity and did not play any role on the pharmacophore model. However, the inversion of C-4 chirality could not be explained by this model.

Dose-response curves for six cembranoids were obtained, four that had produced maximum recovery at 10 μM concentration (**1**, **6**, **10**, and **15**), one with incomplete recovery (**7**) and one inactive (**2**) (Figure 7). The EC_{50}'s of cemranoids with complete recovery (**1**, **6**, **10**, and **15**) correlated well with the QSAR parameter (Figure 7G). This observation strengthens the predicted pharmacophore (Figure 6). Interestingly, the three cembranoids with active oxygens (**1, 6, 10**) have similar Hill coefficients (1.6 to 3.2) while **15** with a sulfur replacing oxygen displayed a very steep curve, clearly different from the others (Figure 7F). This may

be due to the nature of interaction between the oxygen and an electropositive group in the target receptor, which is probably different from that of sulfur. Cembranoid **7**, which produced incomplete recovery, did not correlate with QSAR parameter as the other four (Figure 7G). Cembranoid **7** had a much smaller EC_{50} value than predicted from the QSAR number. It may be because even though it fits well into the hydrophobic zones but it cannot reach the optimal distance from the receptor's electropositive site because of certain rigidity in the 14-membered ring produced by the 7,8 epoxy. Cembranoid **2** showed weak activity at 100 nM, which then disappear at higher concentrations, perhaps because of its binding to a different receptor site that nullifies protection. This interpretation would validate the model assumption that **2** binds (although not very well) to the cembranoids' site and the activity was not observed at 10 μM because of an interfering mechanism.

Finally, these results were particularly satisfactory from the point of view of our long-term goal of designing new druggable analogues of **1**, since out of the relatively small number of tested cembranoids (15), nine active hits were identified with no intrinsic toxicity. The generated pharmacophore model can be applied to discover and design new cembranoid-inspired neuroprotective entities.

3. Experimental

3.1. General Experimental Procedures

The ^{1}H and ^{13}C NMR data were recorded in $CDCl_3$, using TMS as internal standard, on a JEOL Eclipse NMR spectrometer operating at 400 MHz for ^{1}H and 100 MHz for ^{13}C. TLC analysis was carried out on precoated Si gel 60 F254 500 μm TLC plates (EMD Chemicals), using *n*-hexane-EtOAc (1:1) as a developing system. For column chromatography, Si gel 60 (Natland, 63–200 μm) or C18 reversed-phase silica gel (Bakerbond octadecyl 40 μm, Mallinckrodt Baker, Inc., Phillipsburg, NJ) were used. Generally, 1:100 ratios of mixtures to be chromatographed versus the stationary phase were used in all liquid chromatographic purifications. *n*-Hexane-EtOAc (9.5:0.5) with increasing polarity to *n*-hexane-EtOAc (7:3) and isocratic CH_3CN-H_2O (4:6) systems were used for normal and reversed phase chromatography, respectively. A purity of >95% was established for each of **1**-**15** using TLC, HPLC, and/or ^{1}H NMR spectroscopy. All common chemicals and solvents were analytical grade from Sigma-Aldrich (St. Louis, MO).

3.2. Preparation of cembranoids

Compounds **1**-**3** (Supporting Information) were isolated as previously described from fresh tobacco leaf powder (*Nicotiana tabaccum*, Solanacae) purchased from Custom Blends, NY, Blend #28, Batch Number TP-TN-15001, containing Virginia, Oriental, and Burley tobacco (1:1:1).[15] Cembranoids **4** and **8** were semisynthetically prepared by chromic acid oxidation of **3** and **1**, respectively, in dry pyridine.[15,16] Compound **14** was obtained as a minor product in the same reaction starting with **3** (Supporting Information).[15] Cembranoid epoxides **5**-**7** (Supporting Information) were prepared semisynthetically starting with **3** using either *m*-chloroperbenzoic acid in CH_2Cl_2 or metal-catalyzed using vanadyl acetylacetonate, *t*-butyl hydroperoxide in dry toluene.[15] Compound **9** was obtained by biocatalytic transformation of **1** using the symbiotic marine bacterium *Bacillus* sp. NK7.[16] Compounds **10**-**13** (Supporting Information) were also biocatalytic products of **1** using the marine bacterium *Bacillus* sp. NC5.[16] Compound **15** was obtained by reflux of **4** with Lawesson's reagent in toluene.[15]

3.3. Slice preparation and electrophysiological recordings

The preparation of acute hippocampal slices and recording of population spikes (PSs) were done as reported previously.[6,17] Briefly, acute hippocampal slices were prepared from male Sprague Dawley rats (120–200 g) from our colony. All procedures involving animals were

reviewed and approved by the Institutional Animal Care and Use Committee of Universidad Central del Caribe, School of Medicine. A standard artificial cerebrospinal fluid (ACSF), containing (in mM) 125 NaCl, 3.3 KCl, 1.25 NaH_2PO_4, 2 $MgSO_4$, 2 $CaCl_2$, 25 $NaHCO_3$, and 10 glucose, was used for dissection and incubation. Hippocampi were dissected at ice temperature. Transverse slices were cut 400 μm in thickness with a manual slicer and immediately transferred to the recording chamber, which contained three lanes with independent perfusion lines exposed to the same gaseous phase. The lower part of the chamber was filled with H_2O kept at 37.4 ± 1 °C and continuously bubbled with 95% O_2, 5% CO_2. The slices were kept at the gas–liquid interface, on an acrylic plate covered with nylon mesh (Hanes) located above the H_2O superfused with ACSF and kept at 34 ± 1 °C. Before entering the chamber, the ACSF was continuously bubbled with 95% O_2, 5% CO_2 and warmed by flowing through a stainless steel capillary immersed in the lower part of the chamber. The exterior of the chamber was kept at 30 ± 1 °C. The temperature at the three levels (outside, nylon mesh, and water bath) was strictly controlled to minimize variability. The electrophysiological activity of the slices stabilizes one hour after dissection. At that time, PSs were determined in each slice. A concentric bipolar electrode placed in the stratum radiatum of the CA1 area was used to stimulate the Schaffer collateral-commissural fibers with a constant current for 0.2 msec. The PSs were recorded in stratum pyramidale using a glass micropipette filled with 2 M NaCl with impedance ranging from 1 to 5 M. The areas of the PS (millivolts per millisecond) were acquired and analyzed with the Labman program (gift from Dr. T.J. Teyler WWAMI Medical Education Program, University of Idaho, Moscow, ID).

3.4. Procedure for testing neurotoxicity

The procedure used to test neurotoxicity was described earlier and modified by our group.[17-19] About 25-30 slices from two rats were distributed at random among the three lanes. Testing of slices started 1 h after dissection. Each slice was stimulated with a stimulus strength twice that required for eliciting a threshold PS. This initial PS was recorded and compared with the response elicited by the same stimulus, recorded from the same position, after the completion of the experimental treatment. Cembranoids stock solutions were prepared in 100% DMSO and diluted in buffer the day of the experiment; final DMSO concentration was <0.1% v/v; at this concentration, DMSO had no effect on the PSs. To avoid any possible bias associated with the lanes the experimental treatments were rotated among lanes in successive experiments.

Statistical analysis—The data were expressed as % recovery of the PS calculated by dividing the final PS area by the initial PS area in the same slice, and multiplying by 100. The % recovery for each experimental group were compared with the expected 90% recovery due to normal rundown, using One-Sample t-test with the hypothesized population mean equal to 90. The % recovery data from the three experimental conditions were compared among themselves using one-way-ANOVA followed by Student-Newman-Keuls (SNK) multiple comparison method whenever the data passed the normality and equal variance tests; otherwise, Kruskal-Wallis oneway ANOVA on ranks was used followed by the SNK test. Statistical analysis was done using SigmaPlot11.0 graphing software from SYSTAT.

3.4. Common Feature Pharmacophore Model Generation

The two-dimensional (2D) chemical structures of the cembranoids were sketched using ChemDraw Ultra and saved in MDL-molfile format. Subsequently, they were imported into CATALYST, converted into corresponding standard 3D structures and energy minimized to the closest local minimum using the molecular mechanics CHARMm force field implemented in CATALYST. Accordingly, the conformational space of each inhibitor was

explored adopting the “best conformer generation” option within CATALYST, which is based on the generalized CHARMm force field implemented in the program. Default parameters were employed in the conformation generation procedure, i.e., conformational ensembles were generated with an energy threshold of 20 kcal/mol from the local minimized structure and a maximum limit of 250 conformers per molecule.[20-22]

The HipHop-REFINE module of CATALYST software was employed to construct plausible binding hypotheses for cembranoids as nature-derived neuroprotective agents. HipHop-REFINE identifies 3D spatial arrangements of chemical features that are common to active molecules. These configurations are identified by a pruned exhaustive search, starting from small sets of features and extending them until no larger common configuration is found. Active members are evaluated on the basis of the types of chemical features they contain, along with the ability to adopt a conformation that allows those features to be superimposed on a particular configuration. HipHop-REFINE was instructed to explore up to six-featured pharmacophoric space of the following possible features: hydrogen bond acceptor (HBA), hydrogen bond donor (HBD), hydrophobic (Hbic) and positive ionizable. The user defines how many molecules must map completely or partially to the hypothesis via the Principal and MaxOmitFeat parameters. These options allow broader and more diverse hypotheses to be generated.[20,23] HipHop-REFINE uses inactive training compounds to construct excluded volumes that resemble the steric constrains of the binding pocket. It identifies spaces occupied by the conformations of inactive compounds and free from the active inhibitors. These regions are then filled with excluded volumes. HipHop-REFINE was configured to allow a maximum of 10 exclusion spheres to be added to the generated pharmacophoric hypotheses. This represents the default value for the number of excluded volumes in HipHop-REFINE. The following are important HipHop-REFINE control parameters that were used for hypotheses generation:[24]

Spacing: This parameter controls the minimum allowed interfeature distance in the resulting hypotheses. 1.0 Å was employed.

MinPoints: The default value of this parameter is 4, specifying a minimum of four individual feature components for a generated hypothesis.

MinSubset Points: Only configurations of features in input molecules, with at least the number of points specified by this option, are considered when identifying a candidate hypothesis. The default value is 4.

Superposition error, check superposition and tolerance factor: The three control parameters together check the superposition of compounds for hypothesis generation. All three have a default value of 1. Reducing the value from its default tightens the fit.

Misses: This value specifies the number of compounds in the training set that do not have to map to all features in generated hypotheses. One miss was allowed during pharmacophore modeling.

Feature misses: This specifies the number of compounds allowed not to map any particular feature in a generated hypothesis. The default value is 1.

Complete misses: This option specifies the number of molecules that do not have to map to more than one feature per generated hypothesis. In current case this parameter was modified from the default value of zero to 1.

Mapping coefficient: This parameter controls the importance of having compounds with similar structure map to a hypothesis in a similar way. Increasing this parameter will penalize the hypotheses that deviate from this behavior. The default value is 0.

Supplementary Material

Refer to Web version on PubMed Central for supplementary material.

Acknowledgments

The project described was supported by the following grants: NIH-CounterACT U01NS063555 (to PAF), NINDS-SNRP U54NS039408 (to VAE) and NCRR-RCMI Program G12RR03035 (to UCC). ADV was supported by NINDS-SNRP U54NS039408.

References and notes

1. Adigun AA, Wrench N, Seidler FJ, Slotkin TA. Environ Health Perspect. 2010; 118:210. [PubMed: 20123610]
2. Yurumez Y, Durukan P, Yavuz Y, Ikizceli I, Avsarogullari L, Ozkan S, Akdur O, Ozdemir C. Intern Med. 2007; 46:965. [PubMed: 17603234]
3. Newmark J. Arch Neurol. 2004; 61:649. [PubMed: 15148139]
4. Deshpande LS, Carter DS, Blair RE, DeLorenzo RJ. Toxicol Sci. 2010; 116:623. [PubMed: 20498005]
5. Miyaki K, Nishiwaki Y, Maekawa K, Ogawa Y, Asukai N, Yoshimura K, Etoh N, Matsumoto Y, Kikuchi Y, Kumagai N, Omae K. J Occup Health. 2005; 47:299. [PubMed: 16096354]
6. Eterović VA, Perez D, Martins AH, Cuadrado BL, Carrasco M, Ferchmin PA. Toxicol In Vitro. 2011; 25:1468. [PubMed: 21569834]
7. Ferchmin PA, Pérez D, Castro-Alvarez W, Penzo MA, Maldonado HM, Eterovic VA. J Neurosci Res. 2013; 91:416. [PubMed: 23280428]
8. Andersen P, Bliss TV, Skrede KK. Exp Brain Res. 1971; 13:208. [PubMed: 5123965]
9. Martins AH, Alves JM, Perez D, Carrasco M, Torres-Rivera W, Eterović VA, Ferchmin PA, Henning U. PlosOne. 2012; 7:e30755.
10. Leveille F, Papadia S, Fricker M, Bell KF, Soriano FX, Martel MA, Puddifoot C, Habel M, Wyllie DJ, Ikonomidou C, Tolkovsky AM, Hardingham GE. J Neurosci. 2010; 30:2623. [PubMed: 20164347]
11. Ferchmin, P.; Alves, JM.; Perez, D.; Cuadrado, B.; Carrasco, M.; Velez Roman, JM.; Martins, HAB.; Segarra, AC.; Eterović, VA. 2011 Neuroscience Meeting Planner. Washington, DC: Society for Neuroscience; 2011. Program No. 366.09Online
12. Ferchmin PA, Hao J, Perez D, Penzo M, Maldonado HM, Gonzalez MT, Rodriguez AD, de Vellis J. J Neurosci Res. 2005; 82:631. [PubMed: 16247800]
13. Ferchmin, P.; Perez, D.; Martins, AH.; Cuadrado, BL.; Carrasco, M.; Eterović, VA. 2009 Neuroscience Meeting Planner. Chicago, IL: Society for Neuroscience; 2009. Program No. 434.2Online
14. Ferchmin PA, Pagan OR, Ulrich H, Szeto AC, Hann RM, Eterović VA. Toxicon. 2009; 54:1174. [PubMed: 19281835]
15. Baraka HN, Khanfar MA, Williams JC, El-Giar EM, El Sayed KA. Planta Med. 2011; 77:467. [PubMed: 21049399]
16. El Sayed KA, Laphookhieo S, Baraka HN, Yousaf M, Hebert A, Bagaley D, Rainey FA, Muralidharan A, Thomas S, Shah GV. Bioorg Med Chem. 2008; 16:2886. [PubMed: 18222089]
17. Ferchmin PA, Perez D, Biello M. Brain Res. 2000; 859:273. [PubMed: 10719074]
18. Schurr A, Payne RS, Heine MF, Rigor BM. J Neurosci Methods. 1995; 59:129. [PubMed: 7475243]
19. Schurr A, Payne RS, Rigor BM. Neurochem Int. 1995; 26:519. [PubMed: 7492949]
20. Li, H.; Sutter, J.; Hoffmann, R. Pharmacophore perception, development, and use in drug design. In: Gűner, OF., editor. HipHop: Pharmacophores based on multiple common-feature alignment. International University Line; California: 2000. p. 69-84.
21. Smellie A, Kahn SD, Teig SL. J Chem Info Comput Sci. 1995; 35:285.

22. Smellie A, Teig SL, Towbin P. J Comput Chem. 1995; 16:171.
23. Sutter J, Li J, Maynard AJ, Goupil A, Luu T, Nadassy K. Curr Comput Aided Drug Des. 2011; 7:173. [PubMed: 21726193]
24. HipHop User Guide Version 3.1, Catalyst 4.10. Accelrys Inc; 2005. http://www.accelrys.com/doc/life/catalyst410/help/hipHop/HipHop_23TOC.doc.htm [Accessed 01 May 2013]

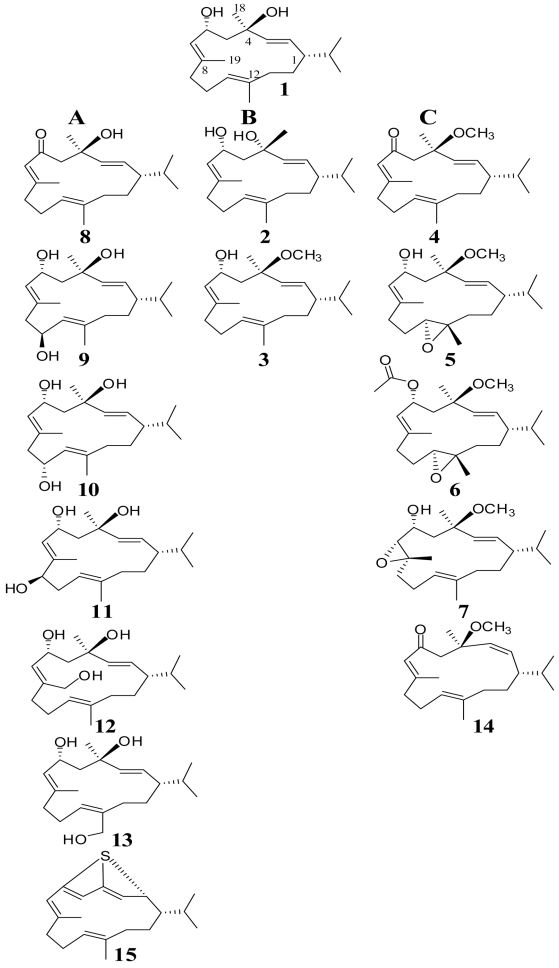

Figure 1.

Structure of natural, semisynthetic and biocatalytic cembranoids tested in this study and correlation between their structures and neuroprotective activity. Tested cembranoids were grouped into three categories: A. Cembranoids with significant protective activity. B. Cembranoids without protective activity. C. Cembranoids with protective activity restored by C-6 keto, C-11*S*,12*S* epoxy, or C-7*R*,8*S* epoxy groups.

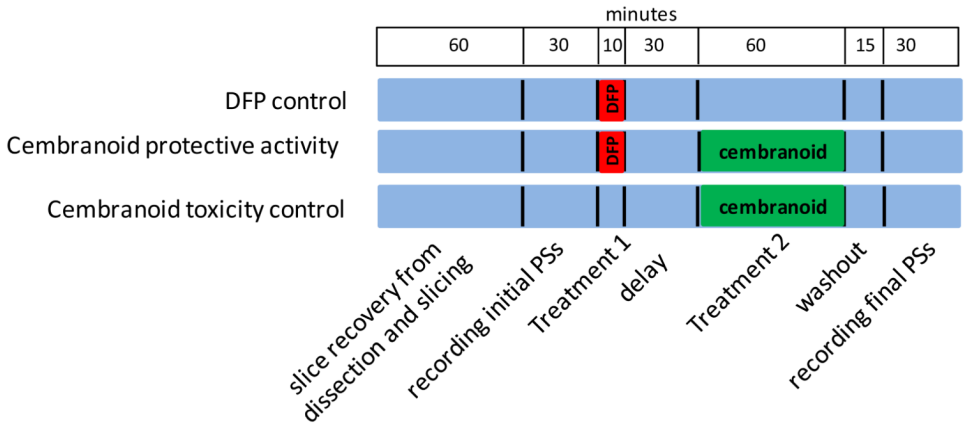

Figure 2.

The experimental protocol. The figure represents the three lanes of the incubation chamber; blue color stands for periods where the slice was superfused with ACSF. There were three treatment groups: 1) *DFP control*, where slices were exposed to 100 μM DFP for 10 min and superfused with ACSF for 105 min before recording the final PSs; 2) *Cembranoid protective activity group*, where slices were exposed to 100 μM DFP for 10 min, washed for 30 min and then exposed to 10 μM cembranoid for 1 h, and 3) *Cembranoid toxicity control*, where slices were exposed to 10 μM cembranoid for 1h.

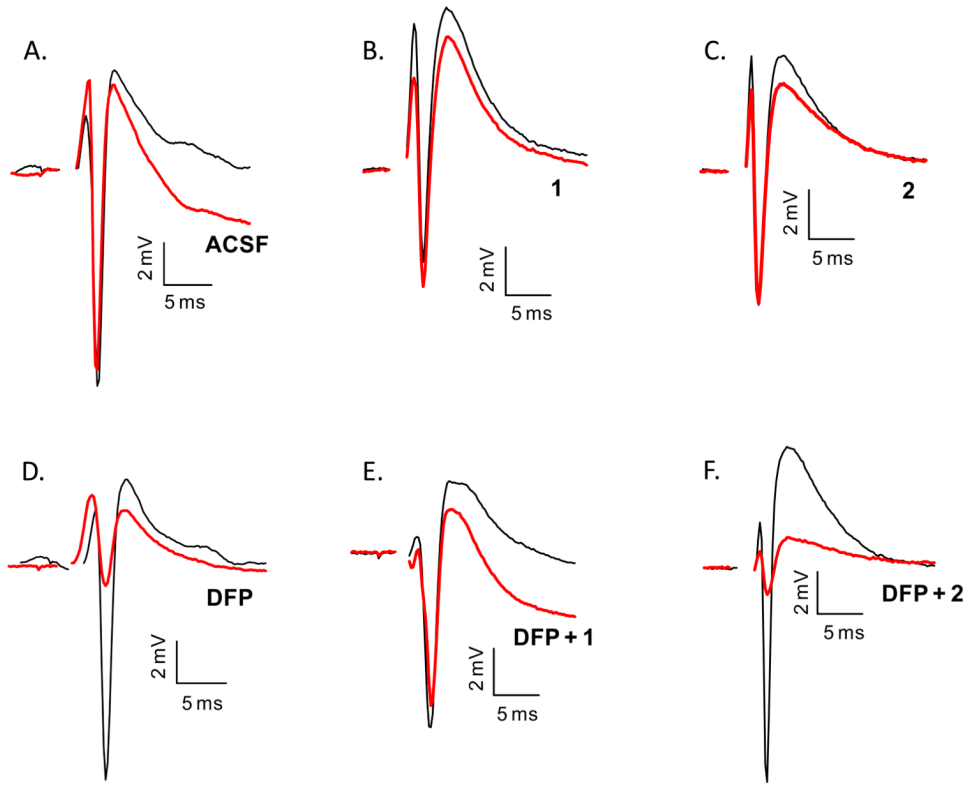

Figure 3.

Representative population spikes recorded after various treatments. Initial PSs (black line) were recorded one-hour after dissection and final PSs (red line) were recorded after treatment as illustrated in Figure 2. A. Initial and final PS for a slice exposed to ACSF for two hours. B. PSs recorded from a slice exposed to 10 μM **1** for 60 min. C. Slice exposed to 10 μM **2** for 60 min. D. PSs recorded from a slice exposed to 100 μM DFP for 10 min. E. PSs recorded from a slice exposed to 100 μM DFP for 10 min followed by a 30 min washout with ACSF and incubation with 10 μM **1** for 60 min. F. Slice exposed to 100 μM DFP for 10 min followed by a 30 min washout with ACSF and incubation with 10 μM **2** for 60 min. Scale bars: vertical, 2 mV; horizontal, 5 ms.

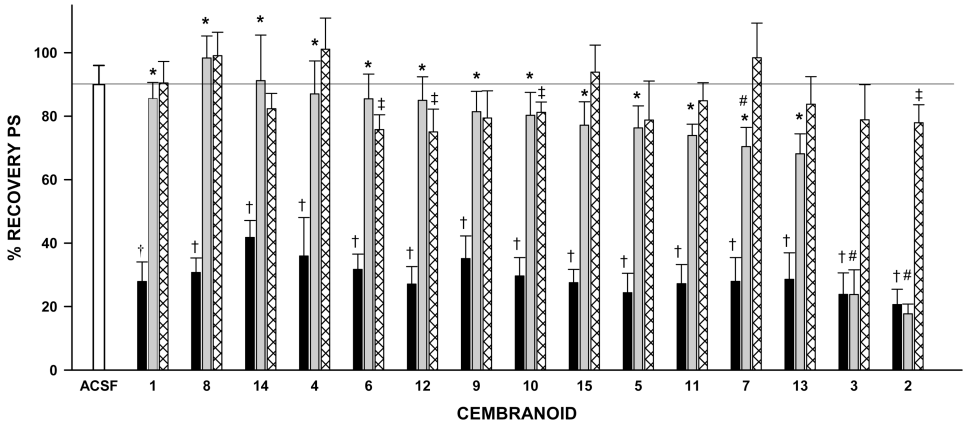

Figure 4.

Neuroprotection by cembranoids. The bars represent the mean±SEM of the % recovery of PSs for the *ACSF control* group (white bar), *DFP control* group (black bars), *Cembranoid protective activity* group (gray bars), and *Cembranoid toxicity controls* (hatched bars) (see Figure 2 for description of groups). The horizontal black line indicates 90% recovery due to rundown of the slice.†: $p<0.001$ for the difference between the % recovery for DFP control and 90% recovery, and ‡: $p<0.05$ for the difference between cembranoid alone and 90% recovery (One-Sample t-test). *: $p<0.01$ for the difference between DFP control and DFP followed by the cembranoid, and #: $p<0.05$ for the difference between DFP followed by the cembranoid and cembranoid alone (one-way-ANOVA followed by Student-Newman-Keuls test). There were two replicate experiments for each analogue, resulting in 14 values per group; three replicates were done for **1** resulting in 21 values per group.

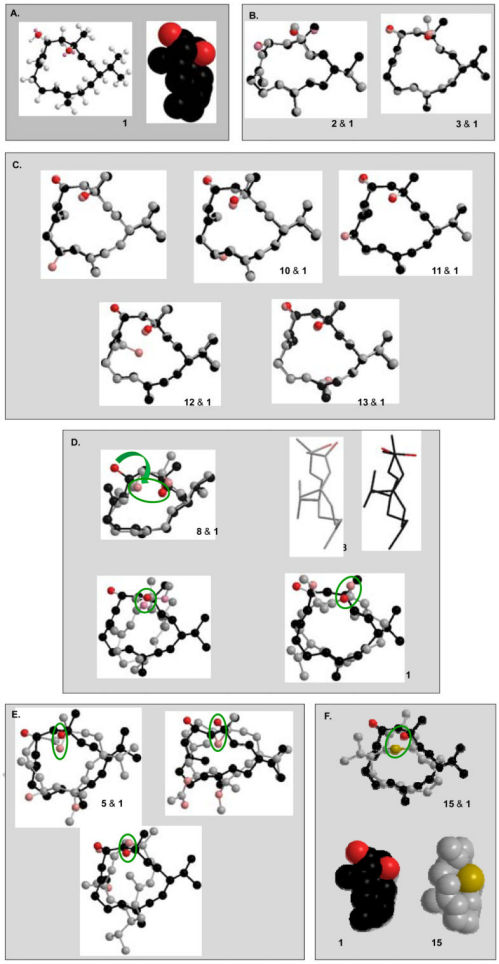

Figure 5.

3D Structure of cembranoids. Energy-minimized 3D structures of cembranoids were obtained using the Chem3D software. In **1**, carbons are depicted in black and oxygen in red. To increase clarity carbons colored gray, oxygen pink, and sulfur yellow. Where indicated, the analogue structure is shown overlapping the structure of **1**.

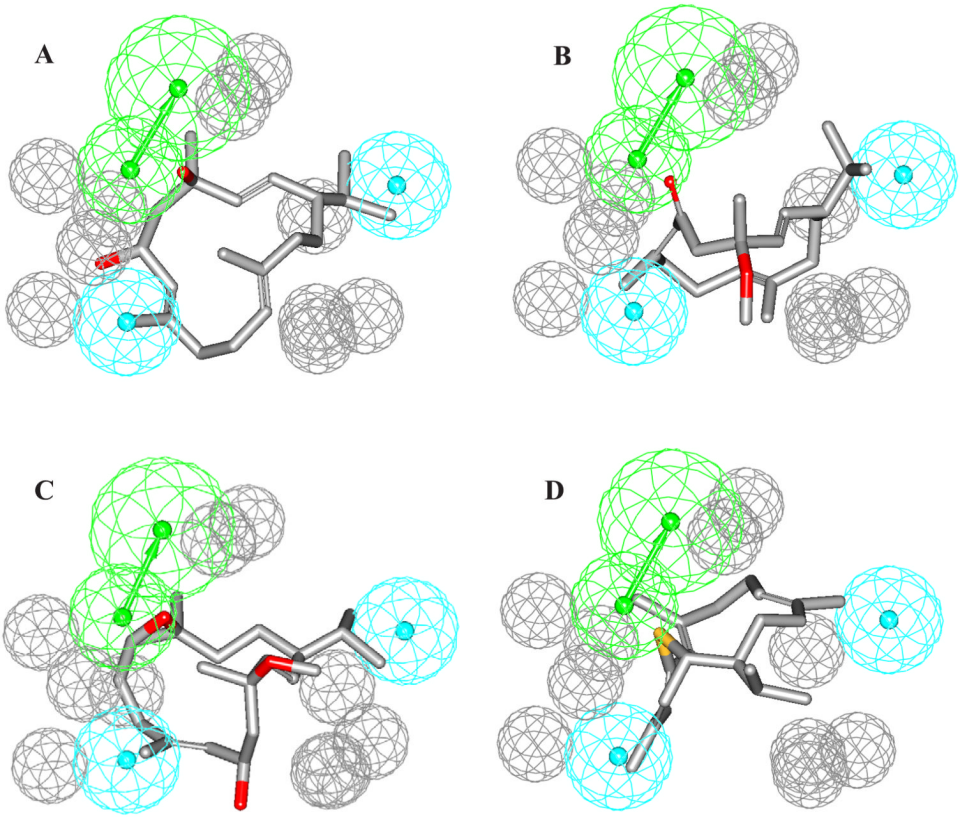

Figure 6.

The highest ranked pharmacophore model of cembranoids as neuroprotective agents and its alignment against (**A**) compound **1**, (**B**) compound **4**, (**C**) compound **5**, (**D**) compound **15**. HBA is depicted as green vectored sphere, hydrophobic features as light blue sphere, and exclusion volumes as gray spheres.

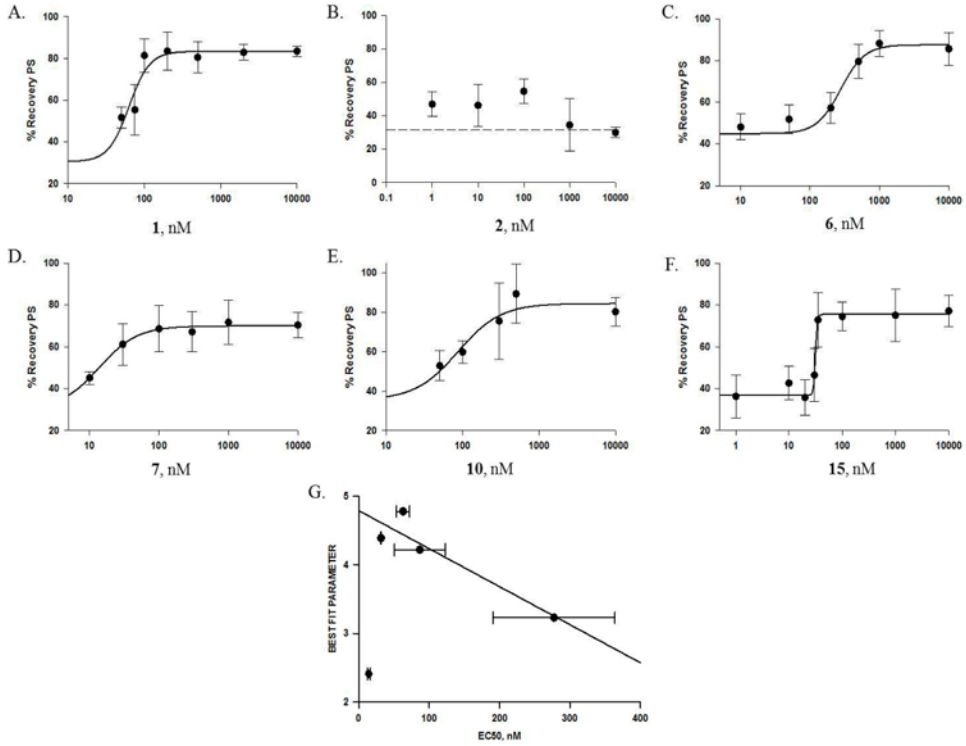

Figure 7.

The concentration-protection curves of representative cembranoids. Panels A-F show the concentration-protection curves for cembranoids: A. **1**, B. **2**, C. **6**, D. **7**, E. **10**, and F. **15**. The experimental protocol was described in General Experimental Procedures and Figure 2; the symbols represent the mean±SEM for the % recovery of the PS after exposure of the slice to DFP followed by the cembranoid at the indicated concentration (n=7-145). In A, C, D, E, and F, the line represents the best fit of the data to the equation: f=min + (max-min)/(1+(x/EC_{50})^(-Hillslope)), with the parameters indicated in Table 1; B. Cembranoid **2** had low activity and could not be fitted to a logistic equation; dashed line represents the % recovery of PS with DFP alone. G. Correlation between the Best Fit QSAR parameters (Table 2) and the EC_{50} values for active cembranoids. A linear correlation was observed for cembranoids **1**, **6**, **10**, and **15** (y_o = 4.8±0.2; slope = -0.0055±0.0015, regression coefficient = 0.93). Cembranoid **7** did not follow the same regression line; it had both smaller EC_{50} and smaller QSAR number compared to other cembranoids in the graph.

Table 1

EC_{50} values of selected cembranoids.

Analogue	Maximum recovery	Minimum recovery	Hill-slope	EC_{50} nM	QSAR
1	83±3	30±6	3.2±1.4	63±9	4.78
2	55±7	32±5	n/a	n/a	1.74
6	88±8	45±4	2.5±1.6	277±87	3.23
7	70±1	30±2	1.6±0.3	14±2	2.41
10	76±2	36±7	1.6±0.9	87±36	4.22
15	85±7	37±2	24.0±10.2	31±1	4.39

Columns 2-5 indicate the parameters for the best fit to the logistic equation f=min + (max-min)/(1+(x/EC50)^ (-Hillslope)), which was used to fit the concentration-protection curves of cembranoids in column 1 (also see Figures 7A-7F). All regression coefficients were > 0.9. The QSAR number is defined in Table 2.

Table 2

The training list used for pharmacophore modeling of cembranoids.

Compounds	Principal value	MaxOmitFeat	Best Fit values against the highest ranked pharmacophore model[a]
1	2	0	4.78
2	0	2	1.74
3	0	2	1.25
4	2	0	3.78
5	2	0	4.44
6	2	0	3.23
7	1	1	2.41
8	2	0	2.47
9	2	0	4.58
10	2	0	4.22
11	2	0	4.91
12	2	0	3.50
13	2	0	3.76
14	2	0	5.01
15	2	0	4.39

[a] Fit values against the pharmacophore, calculated as in the following: Fit = Σmapped hypothesis features × W [1 - Σ (disp/tol)^2], where Σmapped hypothesis features is the number of pharmacophore features that successfully superimpose corresponding chemical moieties within the fitted compound, W is the weight of the corresponding hypothesis feature spheres. This value is fixed to 1.0 in HipHop-generated models. disp is the distance between the center of a particular pharmacophoric sphere and the center of the corresponding superimposed chemical moiety of the fitted compound; tol is the radius of the pharmacophoric feature sphere (known as Tolerance, equals 1.6 Á by default). Σ(disp/tol)^2 is the summation of (disp/tol)^2 values for all pharmacophoric features that successfully superimpose corresponding chemical functionalities in the fitted compound.